Materials Chemistry and Physics 160 (2015) 212–220

Contents lists available at ScienceDirect

Materials Chemistry and Physics

journal homepage: www.elsevier.com/locate/matchemphys

Microstructure and properties of nitrogen ion implantation/AlN/CrAlN/MoS_2-phenolic resin duplex coatings on magnesium alloys

Zhiwen Xie [a, c], Qiang Chen [b, *], Tian Chen [c], Xu Gao [a], Xiaoguang Yu [a], Hua Song [a], Yongjun Feng [a]

[a] University of Science and Technology Liaoning, Anshan 114051, China
[b] Southwest Technique and Engineering Research Institute, Chongqing 400039, China
[c] Chongqing Institute of Green and Intelligent Technology, Chinese Academy of Sciences, Chongqing 400714, China

HIGHLIGHTS

- Ion implantation/AlN/CrAlN/MoS_2-phenolic resin duplex coatings were presented.
- Ion implantation/AlN/CrAlN interlayer greatly enhanced the load bearing capacity.
- Ion implantation/AlN interlayer greatly depressed the effect of galvanic corrosion.
- The AlN/MoS_2-phenolic resin duplex coating showed excellent corrosion resistance.
- The AlN/CrAlN/MoS_2-phenolic resin duplex coating showed super wear resistance.

ARTICLE INFO

Article history:
Received 18 May 2014
Received in revised form
12 February 2015
Accepted 22 April 2015
Available online 4 May 2015

Keywords:
Metals
Coatings
Tribology and wear
Corrosion

ABSTRACT

The novel nitrogen ion implantation/AlN/CrAlN/MoS_2-phenolic resin duplex coatings are fabricated on the AM60 magnesium alloys. The microstructure, tribological and electrochemical properties of the duplex coatings are characterized by X-ray diffraction, X-ray photoelectron spectroscopy, scanning electron microscopy, Fourier transform infrared spectroscopy, Raman spectroscopy, nano-indenter, electrochemical corrosion and wear tester. These studies reveal that the MoS_2-phenolic resin coating has a two-phase microstructure crystalline MoS_2 particles embedded in the amorphous phenolic resin matrix. The single-layer MoS_2-phenolic resin enhances the corrosion resistance of magnesium alloys, but shows poor wear resistance due to the low substrate's load bearing capacity. The addition of nitrogen ion implantation/AlN/CrAlN interlayer in the MoS_2-phenolic resin/substrate system greatly enhances the substrate's load bearing capacity. The AlN/CrAlN/MoS_2-phenolic resin duplex coating with a high load bearing capacity demonstrates super wear resistance (i.e., long wear life and low friction coefficient). In addition, the nitrogen ion implantation/AlN interlayer greatly depresses the effect of galvanic corrosion because its potential is close to that of the magnesium alloys, but the nitrogen ion implantation/AlN/CrAlN interlayer is inefficient in reducing the galvanic corrosion due to the large potential difference between the CrN phase and the substrate. As a result, the nitrogen ion implantation/AlN/MoS_2-phenolic resin duplex coating shows a better corrosion resistance compared to the nitrogen ion implantation/AlN/CrAlN/MoS_2-phenolic resin.

1. Introduction

Magnesium alloys have attracted extensive attention in aerospace and automotive industries due to their outstanding properties, including high strength-to-weight ratio, good damping capacity, and large potential recycling capability [1–5]. Unfortunately, the poor chemical corrosion and wear resistance of magnesium alloys greatly constraints their real applications in engineering fields [6,7]. To overcome these drawbacks, fabricating a protective coating with super anti-wear and anti-corrosion properties has been accepted as one of the most effective methods.

Various coatings have been explored to push magnesium alloys

* Corresponding author. No.33 Yuzhou Road, Chongqing 400039, China.
E-mail address: 2009chenqiang@163.com (Q. Chen).

http://dx.doi.org/10.1016/j.matchemphys.2015.04.026
0254-0584/

to be used in practical engineering applications. Microarc oxidation coatings fabricated on magnesium alloys exhibit a high hardness and an excellent corrosion resistance [8–10]. However, these coatings also have a high friction coefficient and suffer from the pitting corrosion in the through thickness micropores [11,12]. Ion implantation improves the corrosion resistance of magnesium alloys [13–15], but the modified layers are very thin with limited protective effect compared to the thicker ceramic coatings. Hard coatings, such as TiN or CrN, exhibit superior mechanical properties (i.e., high hardness and high adhesion strength) [16–19], whereas galvanic corrosion takes place inevitably in the region of through thickness defects due to the large electrode potential difference between them [18,19]. Diamond-like carbon (DLC) with high hardness, low friction coefficient, and excellent chemical inertness has been studied as anti-wear and anti-corrosion coating of magnesium alloys [20,21], However, the DLC coating has a short wear life and poor adhesion strength to the substrate arising from their different physical properties. Soft phenolic resin-based self-lubricating coatings seem to be a good candidate to act as the protective coating due to their super wear and corrosion resistance [22–24]. However, it is generally believed that soft coatings fabricated on magnesium alloys usually exhibits a poor wear resistance due to the low substrate's load bearing capacity.

These previous studies suggest that a single protective coating is almost impossible to satisfy the requirements of magnesium alloys in anti-wear and anti-corrosion aspects. Multiple-layer coatings are considered to be able to depress the galvanic corrosion and simultaneously provide high load-bearing capacity for soft magnesium alloys. For example, duplex coatings, such as Al/AlN/DLC, display superior properties compared with their single layer counterparts [25–27]. Here, a functional duplex architecture consisting of nitrogen ion implantation, AlN, CrAlN and MoS_2-phenolic resin is designed to improve the wear and corrosion resistance of magnesium alloys. Nitrogen ion implantation is used to induce surface densification and effectively improve the interfacial bonding strength. The AlN or AlN/CrAlN interlayers provide load support for the soft MoS_2-phenolic resin and depress the pitting corrosion process. The outmost MoS_2-phenolic resin layer acts as the protective layer with excellent anti-corrosion and self-lubricating properties. The microstructure, wear and corrosion resistance of the duplex coatings with different interlayers are investigated in details.

2. Materials and methods

Si wafer and AM60 magnesium alloys were used as the substrate. The samples were mechanically polished by diamond paste and ultrasonically washed using pure ethanol. Pure Al (99.9%) and CrAl alloys (50:50 at. %) was used as the targets. High purity argon and nitrogen were used as the working atmosphere. Prior to the coating deposition, all samples were cleaned by argon ion sputtering to remove contaminants and the native oxide layer. Afterwards, the samples were treated by nitrogen ion implantation. The AlN and CrAlN interlayer were synthesized by plasma immersion ion implantation and deposition [28]. The experimental parameter of the sputtering cleaning, nitrogen ion implantation and interlayer fabrication were summarized in Table 1. The top MoS_2-phenolic resin layers were prepared by mechanical spraying. High purity micron-scale MoS_2 powders and phenolic resin were added to the organic solvent in a certain weight ratio. The mixed solutions were dispersed under supersonic agitation for 1 h followed by mechanical spraying. The coated samples were solidified in a sintering furnace. The curing temperature was set at 180 °C for 90 min. The experimental details of the as-fabricated duplex coatings were shown in Table 2.

The crystalline structure of the coatings was determined by an X-ray diffraction (XRD, Philips-X'pert) apparatus using Cu Kα radiation source. The diffraction angle was ranged from 20° to 80°. The chemical bonding of the coatings was investigated by X-ray photoelectron spectroscopy (XPS, Thermo, K-Alpha) using Al Kα radiation ($h\nu = 1486.6$ eV) as the excitation source. Argon ion etching was performed to remove contaminants with an accelerating voltage of 1000 eV. Scanning electron microscopy (SEM, JSM-6701F) was employed to observe the surface and cross-section morphologies of the coatings. Raman spectrometer (Renishaw inVia, $\lambda = 532$ nm) was used to identify the structure of the MoS_2-phenolic resin coating. Fourier transform infrared spectroscopy (FTIR, Nicolet) was used to indentify the chemical bonding status in the MoS_2-phenolic resin coating. A ball-on-disc wear tester (MFT-R4000) was used to characterize wear resistance performance of the samples. A 5 N load was applied onto the sample through a 6 mm Si_3N_4 ball. The sliding distance and the frequency was 5 mm and 2 Hz, respectively. The wear test was evaluated in the ambient atmosphere with a relatively humidity of 35% and a temperature of 25 °C. The friction test was performed three times under the same conditions to evaluate the reliability of the measurements. The mechanical properties of the samples were determined by using a nano-indentation system. The hardness and elastic modulus were calculated according to the Oliver-Pharr method. The electrochemical properties of the samples were evaluated by electrochemical tests (PGSTAT302N). The three-electrode electrochemical system included a high purity platinum needle as the counter cathode, being measured sample as the working electrode (1 cm^2 exposed areas), and a saturated calomel electrode (SCE) as the reference electrode. The test was carried out in a 1 M NaCl solution. All electrochemical tests were conducted for three times to ensure the reproducibility. The elemental composition of the wear tracks and the corrosion morphologies were examined by scanning electron microscope (SEM) equipped with energy dispersive spectrometer (EDS).

3. Results and discussion

3.1. Microstructure characterization of the as-fabricated coatings

Fig. 1a shows the XRD patterns of the substrate, nitrogen implanted substrate, nitrogen ion implantation/AlN interlayer and nitrogen ion implantation/AlN/CrAlN interlayer. After removing the substrate signals from XRD patterns, the AlN (002) peak identified in the nitrogen implanted substrate and nitrogen ion implantation/AlN interlayer, which is in agreement with the previous studies that the AlN films present the (002) preferred texture [25,29]. In addition, a weak AlN (002) peak and a strong CrN (200) peak are identified in the nitrogen ion implantation/AlN/CrAlN interlayer. It has been reported that the solubility of Al in cubic CrN can reach 70% [30], which implies that Cr atoms tends to be replaced by Al atoms to form cubic CrAlN solid solution in the as-deposited CrAlN layer. Fig. 1b shows the XRD pattern of the MoS_2-phenolic resin coating. The diffraction peaks located at 14.32°, 29.02°, 32.68°, 35.89°, 39.49°, 44.15°, 49.79°, 60.17°, 70.14° and 88.71° are associated with diffraction form (002), (004), (100), (102), (103), (006), (105), (008), (108) and (118) crystal planes of the MoS_2, respectively, proving the formation of MoS_2 crystals in the MoS_2-phenolic resin layer.

The high resolution XPS spectra of the AlN interlayer are shown in Fig. 2. The binding energy of Al2p peak presented in Fig. 2a locates at 74.3 eV, which can be assigned to the Al signal from AlN [25,31]. As shown in Fig. 2b, the binding energy of N1s peak centers at 396.9 eV, which is associated with the Al–N bond [25,32].

Fig. 3a shows the SEM surface image of the sample A1, from

Table 1
Experimental parameters of the duplex coatings.

	Sputtering cleaning	Ion implantation	AlN layer	CrAlN layer
N_2 flow rate (sccm)	–	50	50	50
Ar flow rate (sccm)	50	–	–	–
RF power (W)	600	600	–	–
Partial Pressure (Pa)	0.6	0.6	0.3	0.3
Cathode duration time (μs)	–	–	3000	3000
Bias voltage (kV)	−6	−30	−20	−20
Bias voltage duration time (μs)	60	20	60	60
Frequency (Hz)	100	200	50	50
Time (h)	0.5	2	2	2

Table 2
Experimental details of the duplex coatings.

Sample	Coating
A0	AM60 substrate
A1	Single-layer MoS_2-phenolic resin
A2	Nitrogen ion implantation/AlN/MoS_2-phenolic resin
A3	Nitrogen ion implantation/AlN/CrAlN/MoS_2-phenolic resin

which we can see a uniform surface coating dispersed with numerous micrometer-sized particles. The average thickness of the sample A1 is about 11.771 μm (Fig. 3b). In addition, some visible micro-pores are also observed on the surface and in the cross-section images of the sample A1. Sample A2 has a two-layer structure and the thickness of the AlN interlayer is 350 nm (Fig. 3c). Three-layer structure is observed for sample A3 and the thickness of the AlN/CrAlN interlayer is 800 nm (Fig. 3d).

Fig. 4 shows the FTIR spectrum of the MoS_2-phenolic resin coating. The vibration peak located at 1121.77 cm^{-1} originates from the O—H groups. The band centered at 1384.45 cm^{-1} corresponds to C—C groups. The peaks located at 2923.10 cm^{-1} and 2853.33 cm^{-1} are assigned for the C—H_2 and C—H groups, respectively. The bands located at 1638.11 cm^{-1}, 720.44 cm^{-1}, 578.36 cm^{-1} and 462.07 cm^{-1} are contributed by the different vibration modes of the benzene rings. These above results confirm that the nitrogen ion implantation/AlN/CrAlN/MoS_2-phenolic resin

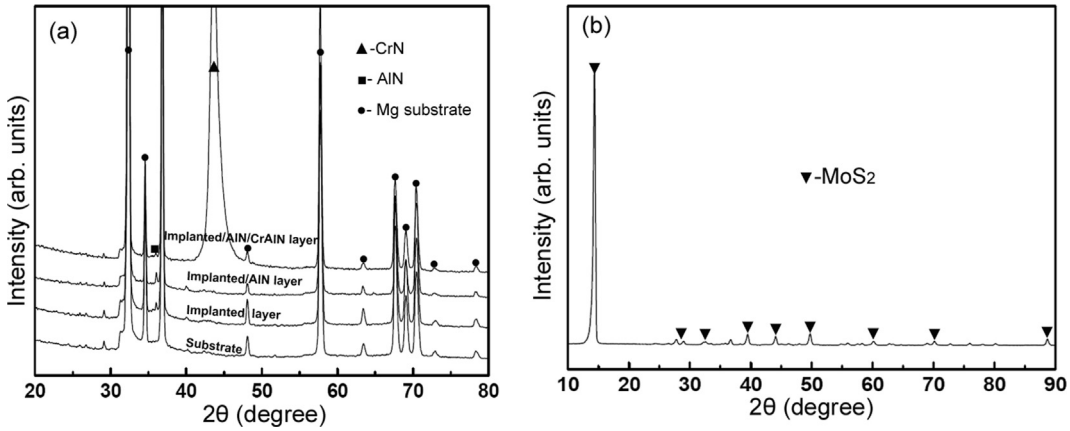

Fig. 1. (a) XRD patterns of the substrate, nitrogen implanted substrate, nitrogen ion implantation/AlN interlayer and nitrogen ion implantation/AlN/CrAlN interlayer, (b) XRD pattern of the MoS_2-phenolic resin coating.

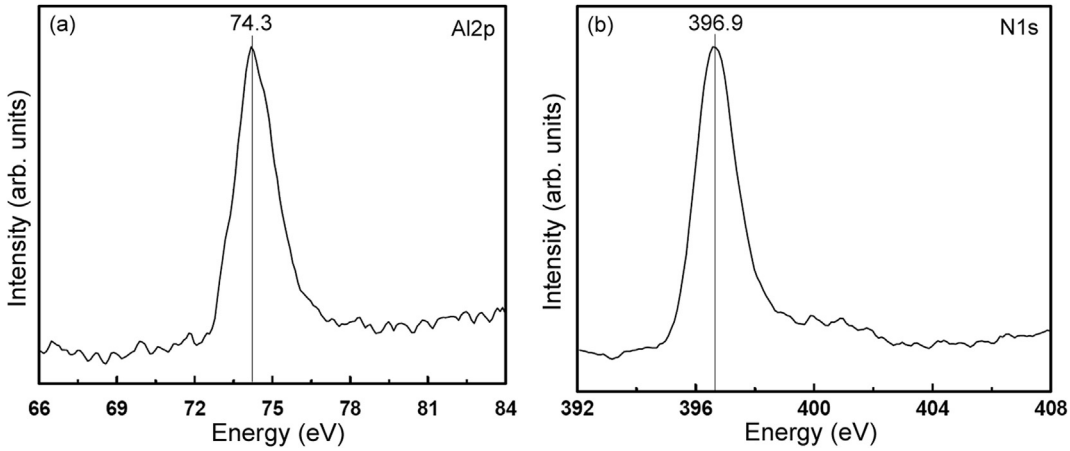

Fig. 2. High resolution XPS spectra of the AlN interlayer: (a) Al2p, (b) N1s.

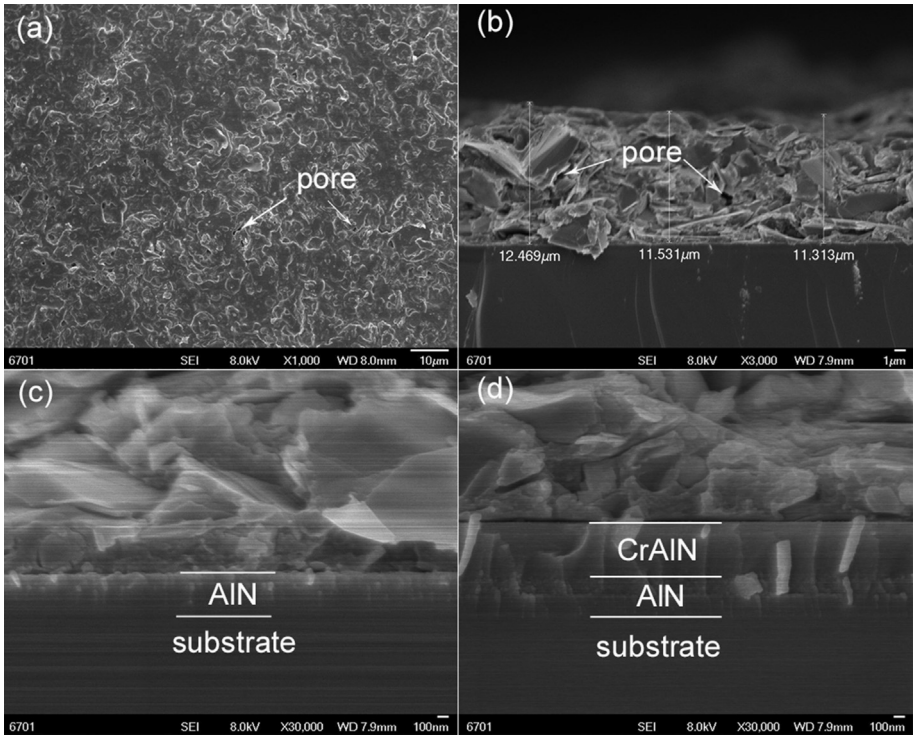

Fig. 3. (a) SEM surface and (b) cross-section images of the sample A1, (c) SEM cross-section image of the sample A2, (d) SEM cross-section image of the sample A3.

duplex coatings are successfully fabricated on the nitrogen implanted magnesium alloys.

3.2. Tribological performance of the as-fabricated coatings

Fig. 5 shows the friction curves of the samples. The friction coefficient of sample A0 is as high as 0.45. A strong fluctuation of the friction coefficient can be observed during the friction test (Fig. 5a). Sample A1 has a low friction coefficient of 0.15 at the initial stage, and then increases from 0.15 to 0.28 as the sliding time reach 22 min, indicating that this coating has been worn out gradually (Fig. 5b). Sample A2 also remains a stable friction coefficient of 0.13 at the initial stage, and subsequently fluctuates strongly when the sliding time is greater than 58 min (Fig. 5c). In comparison to sample A2, sample A3 exhibits a low and stable friction coefficient of 0.09 during the whole friction test, indicating its superior wear resistance performance (Fig. 5d).

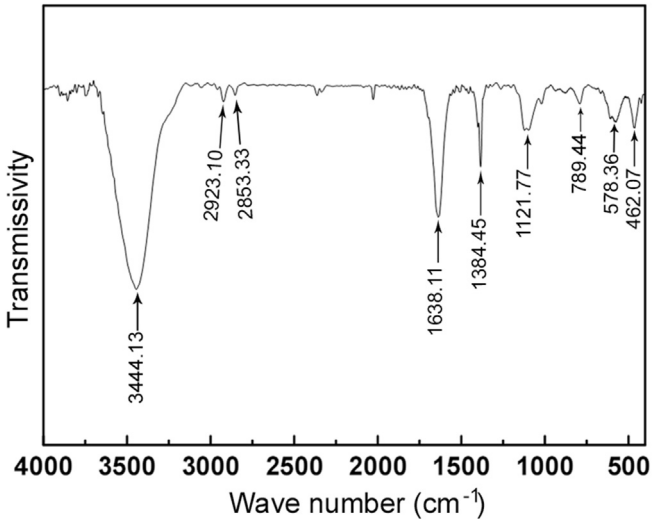

Fig. 4. FTIR spectrum of the MoS_2-phenolic resin coating.

Fig. 6a shows the wear track Raman spectrum of the sample A2 at the wear track locations. The peaks located at 380.61 cm^{-1} and 408.16 cm^{-1} are assigned to the MoS_2 [33]. The peak located at 610.68 cm^{-1} corresponds to the A (TO) mode of the AlN film [34]. The corresponding wear track image in the inset of Fig. 6a shows that a small amount of MoS_2-phenolic resin debris exists on the wear track surface, evidencing that the outmost MoS_2-phenolic resin layer tends to be worn out. Additionally, some visible cracks are observed at the wear track edges, resulting from the low load carrying capacity of the AlN interlayer. The wear track Raman spectrum of the sample A3 at the wear track sites presented in Fig. 6b shows that only MoS_2 peaks are identified in the wear track. SEM image of the wear track shown in the inset in Fig. 6b reveals that sample A3 has a smooth surface at the wear track area, indicating the excellent wear resistance of this coating.

Fig. 7 shows the wear track morphologies with the corresponding EDS spectra of all samples. As shown in Fig. 7a, the wear track of the sample A0 is featured by a great number of ploughs. Sample A1 has very similar wear track morphology to that of the sample A0 (Fig. 7b). The corresponding EDS spectrum reveals that no S and Mo are identified in the wear track, indicating that this coating has been worn out. However, sample A2 displays a smooth surface in the wear track with some visible cracks (Fig. 7c). The Al content in the wear track of sample A2 is higher than that of sample A0 as proved by the EDS spectrum, underlying that the AlN interlayer has not been wear out. Although a small amount of S and Mo elements also appears in the wear track, the outmost MoS_2-phenolic resin layer tends to be peeled off reflected by the strong fluctuation in the friction coefficient (Fig. 5c) and the morphology of the wear track shown in the inset in Fig. 6a. Sample A3 bears a

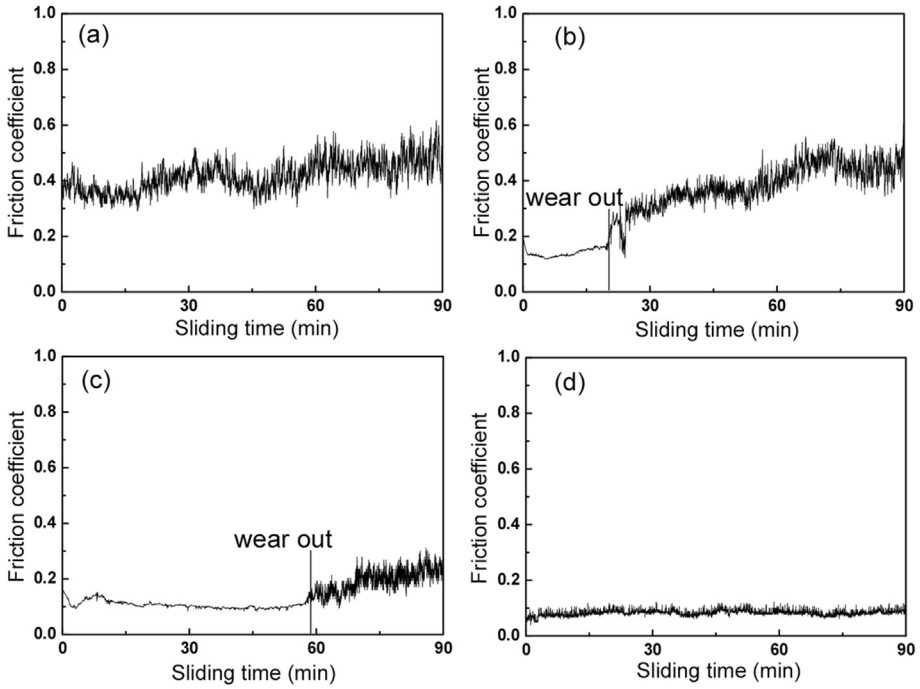

Fig. 5. Friction curves of all samples: (a) A0, (b) A1, (c) A2, (d) A3.

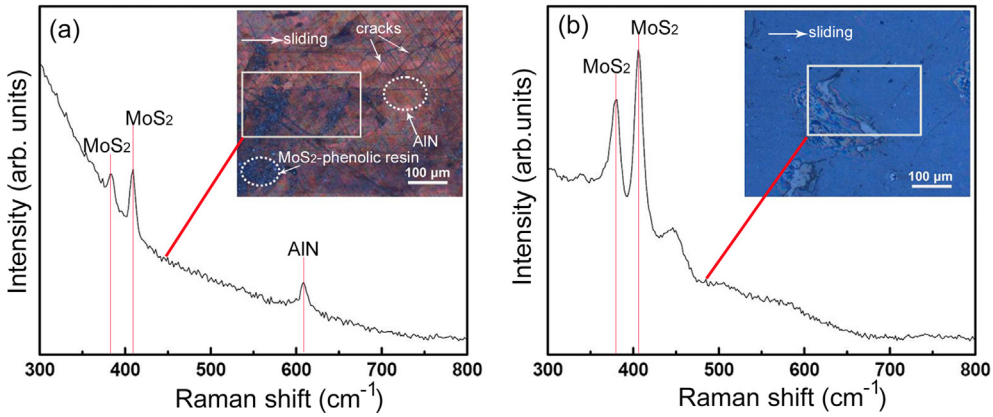

Fig. 6. Wear track Raman spectra of (a) the sample A2 and (b) sample A3.

smooth surface in the wear track region (Fig. 7d). Only Mo and S elements are observed in the wear track proved by the corresponding EDS spectrum, suggesting that the outmost MoS_2-phenolic resin layer is intact after the wear resistance test.

It has been reported that MoS_2 has a layered sandwich structure and tends to form a lubrication transfer film on the counter face under a shearing forces [35]. The typical morphology of the mating ball with the corresponding EDS spectrum of the sample A3 is shown in Fig. 8. A large amount of debris is observed on the wear scar surface of the mating ball. Strong S and Mo signals are identified in the wear scar surface in the corresponding EDS spectrum. These above results conform that the self-lubricating property of the as-fabricated duplex coatings arises from the formation of a MoS_2 lubrication transfer film by the outmost MoS_2 during the friction period.

Fig. 9 shows the cross-section wear track profiles of all samples. As shown in Fig. 9a, the width and depth of the wear track in sample A0 are 1.59 mm and 120.51 μm, respectively, which are wider and deeper in comparison to that in sample A1 (723.25 μm and 28.23 μm, respectively, Fig. 9b). The width and depth of the wear track in sample A2 is 493.37 μm and 11.57 μm, respectively (Fig. 9c). In comparison, sample A3 exhibits the smallest wear track width (412.21 μm) and wear track depth (7.13 μm), exhibiting the best performance in wear resistance (Fig. 9d).

It has been reported that the wear life of soft coatings largely depends on the substrate's load bearing capacity [36,37], and a higher substrate's hardness generally corresponds to a better wear resistance. Fig. 10 shows the nanoindentation results of all samples. Sample A0 has a hardness of 0.93 GPa and a modulus of 34.52 GPa (Fig. 10a). The hardness and modulus are 1.95 GPa, 51.23 GPa for MoS_2-phenolic resin coating (Fig. 10b) and 4.72 GPa, 69.25 GPa for the nitrogen ion implantation/AlN interlayer (Fig. 10c), respectively. The nitrogen ion implantation/AlN/CrAlN interlayer exhibits a high hardness of 16.95 GPa and a high modulus of 175.12 GPa (Fig. 10d), showing a strong load-bearing capacity.

According to the tribological and mechanical results, a single

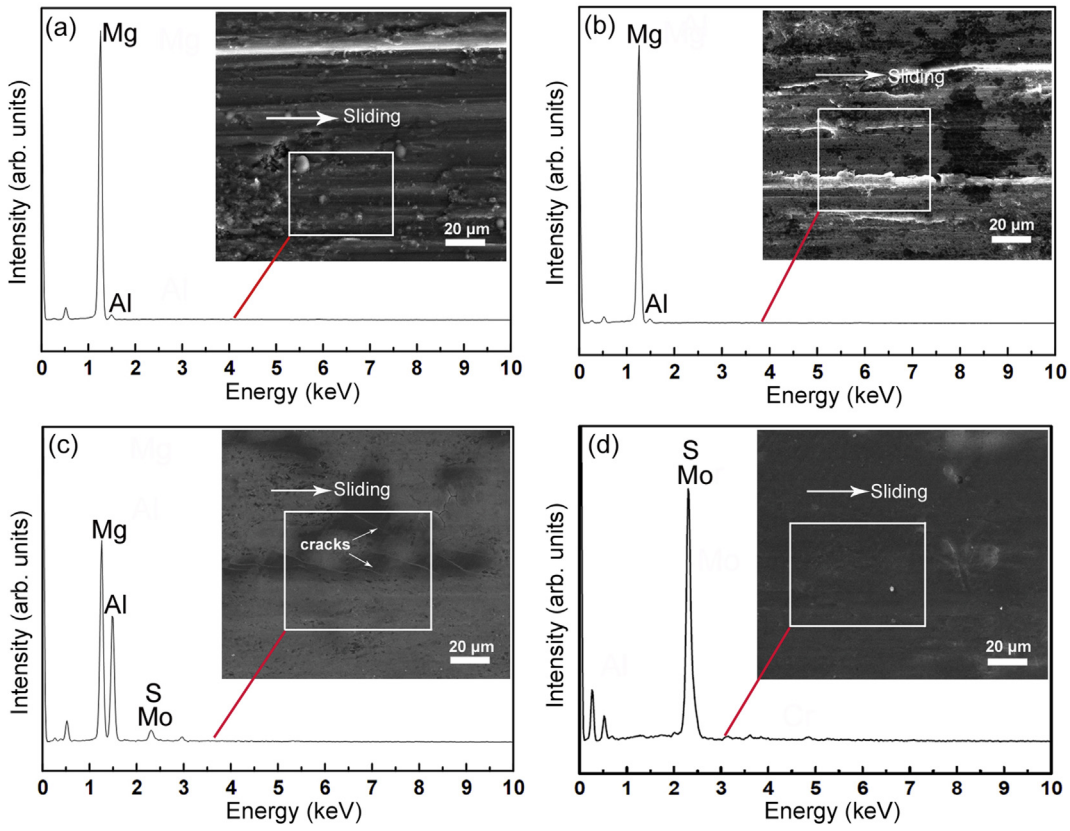

Fig. 7. Wear track morphologies with the corresponding EDS spectra of all samples: (a) A0 (b) A1, (c) A2, (d) A3.

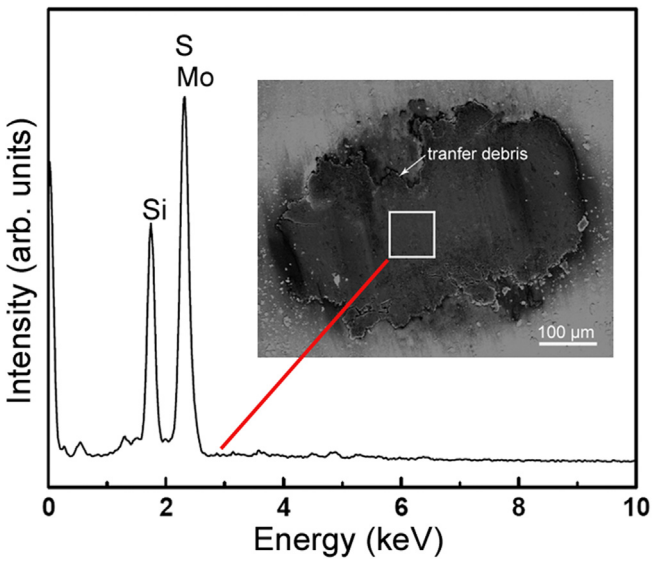

Fig. 8. The typical morphology of the mating ball with the corresponding EDS spectrum of the sample A3.

layer of the MoS_2-phenolic resin coating shows a poor wear resistance, which can be attributed to the low load-bearing capacity of magnesium alloys. In contrast, the as-fabricated duplex coatings exhibit improved wear resistance with prolonged wear life as the thickness of the interlayer increases. The improved performance benefits from the enhancement of the substrate's load-bearing capacity. As shown in Fig. 10c, the nitrogen ion implantation/AlN interlayer has a low hardness and can not supply sufficient support during the friction period. The limited bearing capacity of the AlN interlayer generates numerous cracks distributed along the wear track boundaries (Figs. 6a and 7c), which leads to unsatisfactory wear life of sample A2 (Fig. 5c). In comparison, the nitrogen ion implantation/AlN/CrAlN interlayer possesses a high hardness and provides adequate load support for the soft magnesium alloys. The high load bearing capacity of the interlayer contributes the superior wear resistance of sample A3 (Fig. 5d).

3.3. Electrochemical corrosion behaviors of the as-fabricated coatings

Fig. 11 shows the anode polarization curves of all samples. Sample A0 has a corrosion potential of −1.39 V and a corrosion current density of 8.89×10^{-5} A/cm^2. Sample A1 shows improved corrosion resistance compared with sample A0 with a corrosion potential of −1.15 V and a corrosion current density of 6.05×10^{-7} A/cm^2. The corrosion potential and corrosion current density of sample A2 are −1.23 V and 2.31×10^{-9} A/cm^2, respectively. As to sample A3, the corrosion takes place at −1.01 V with the current density of 5.12×10^{-7} A/cm^2, respectively. Electrochemical test results demonstrate that the corrosion resistance of magnesium alloys is improved significantly by the nitrogen ion implantation/AlN/MoS_2-phenolic resin duplex coating.

The morphologies of the samples after corrosion are shown in Fig. 12. A large amount of corrosion defects (e.g., cracks and pores) is observed on the surface of sample A0 because of the severe corrosion degradation. Compared with sample A0, very few corrosion products and defects are observed on the surface of sample A1 and A2, indicating that these coatings have excellent

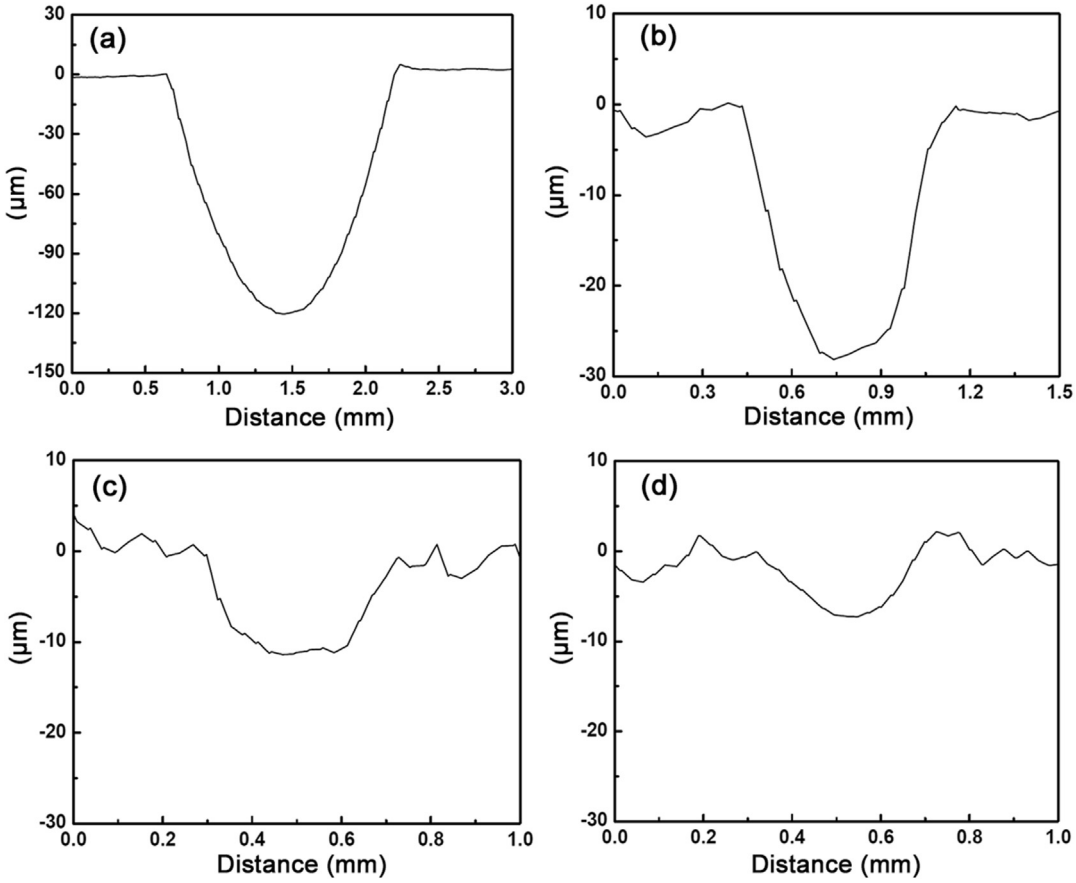

Fig. 9. Cross-section wear track profiles of all samples: (a) A0, (b) A1, (c) A2, (d) A3.

corrosion resistance (Fig. 12b and c). Loose surface morphology is the main feature of sample A3 with some visible cracks, implying the deteriorative corrosion resistance (Fig. 12d).

Previous studies have proved that pitting corrosion can destroy the protective coating starting from those through thickness defects [11,12]. The local galvanic corrosion is also inclined to occur in the region of these defects because of the large potential difference between the coating and the underneath substrate. For instance, Wu [18] reported that the Cr/CrN interlayer did not improve the corrosion resistance of the DLC/AZ31 system due to the formation of galvanic cell between the interlayer and the substrate. The galvanic corrosion can be greatly depressed when the potential of the interlayer is close to that of the magnesium alloys [38,39]. According to these previous studies, MoS_2-phenolic resin coating can improve the corrosion resistance of magnesium alloys, but these micro-pores in the coating are most likely as diffusion channels of the corrosive media. The introduction of nitrogen ion implantation/AlN interlayer between the MoS_2-phenolic resin and the substrate greatly depresses the galvanic corrosion. As studied in the reference

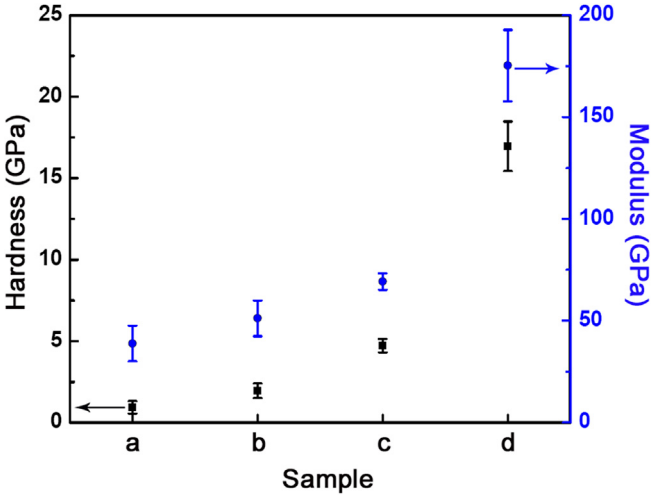

Fig. 10. Nanoindentation results of all samples: (a) magnesium alloy, (b) MoS_2-phenolic resin coating, (c) nitrogen ion implantation/AlN interlayer, (d) nitrogen ion implantation/AlN/CrAlN interlayer.

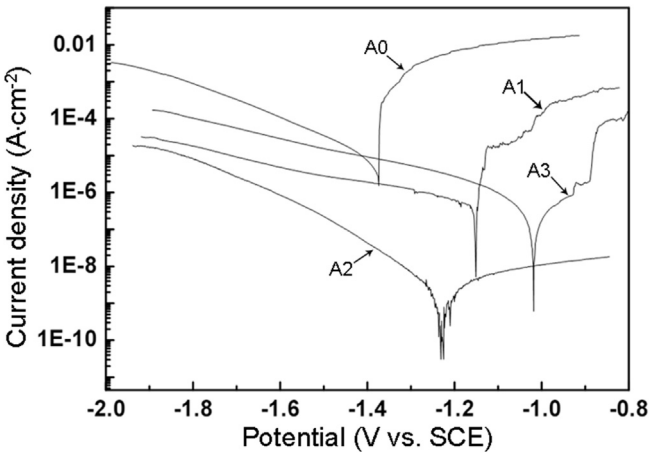

Fig. 11. Potential dynamic polarization curves of all samples.

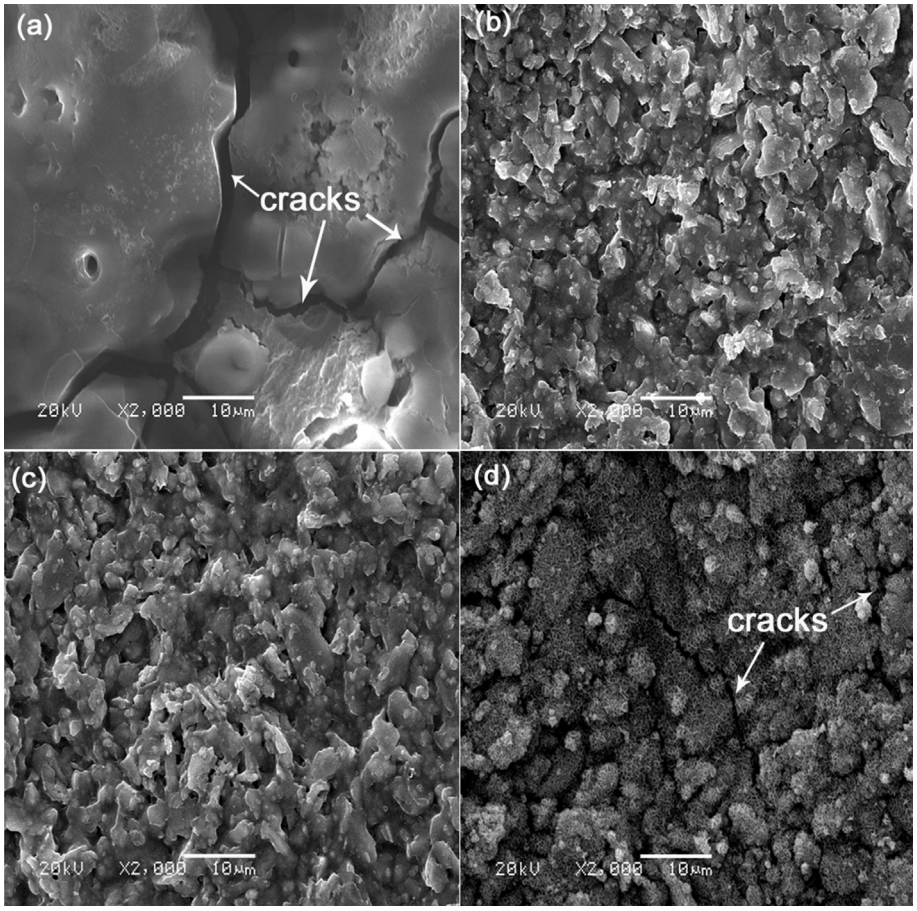

Fig. 12. Corrosion morphologies of all samples: (a) A0, (b) A1, (c) A2, (d) A3.

[40], ion implantation induces surface densification and the formation of a thin AlN near the surface, both of which benefit the corrosion resistance improvement of magnesium alloys. The AlN interlayer reduces the effect of galvanic corrosion because its potential is close to that of the substrate [25]. As a result, the nitrogen ion implantation/AlN/MoS_2-phenolic resin duplex coating shows a better corrosion resistance compared to the single-layer MoS_2-phenolic resin coating. However, the nitrogen ion implantation/AlN/CAlN interlayer can not enhance the corrosion resistance of the coating/substrate system due to the large potential difference between the CrN phase and the substrate [18]. As shown in the references [6,19], it is nearly impossible to prohibit the formation of pinholes in PVD coatings. These defects in the AlN/CrAlN layer can behave as diffusion channels of the corrosive media, inducing the galvanic corrosion between the substrate and the CrN phase. Therefore, the corrosion resistance of the nitrogen ion implantation/AlN/CrAlN/MoS_2-phenolic resin duplex coating is weakened.

4. Conclusions

(1) The MoS_2-phenolic resin coating has a two-phase composite structure which is the MoS_2 crystalline embedded in the phenolic resin matrix.
(2) Fabrication of MoS_2-phenolic resin coating on magnesium alloys can improve their corrosion resistance performance, but it does not benefit their wear resistance improvement due to the low load bearing capacity of magnesium alloys.
(3) Introduction of nitrogen ion implantation/AlN/CrAlN interlayer between MoS_2-phenolic resin layer and substrate remarkably enhance the load bearing capacity of magnesium alloys. The nitrogen ion implantation/AlN/CrAlN/MoS_2-phenolic resin duplex coating with enhanced load bearing capacity exhibits good performance in wear resistance.
(4) The nitrogen ion implantation/AlN interlayer effectively depresses the galvanic corrosion. However, the nitrogen ion implantation/AlN/CrAlN interlayer is inefficient in enhancing the corrosion resistance of the coating/substrate system due to the large potential difference between the CrN phase and the substrate. The nitrogen ion implantation/AlN/MoS_2-phenolic resin duplex coating exhibits a better corrosion resistance in comparison to the nitrogen ion implantation/AlN/MoS_2-phenolic resin duplex coating.

Acknowledgement

This work is supported by the National Natural Science Foundation of China (No. 51401201) and Chinese Academy of Sciences Western Light (No. Y32Z010F10) and Chongqing Research of Application Foundation and Advanced Technology (No. cstc2014jcyjA50009) and Enterprise Cooperation Project (No. Y32H130F10). We gratefully acknowledge Prof. L. P. Wang, Harbin Institute of Technology, for helpful discussions and contributions during the coating preparation.

References

[1] Hassan Jafaria, Mohd Hasbullah Idris, Ali Ourdjini, Mohammed Rafiq Abdul Kadir, An investigation on interfacial reaction between in-situ melted

AZ91D magnesium alloy and ceramic shell mold during investment casting process, Mater. Chem. Phys. 138 (2013) 672–681.
[2] Q. Chen, S.J. Luo, Z.D. Zhao, Microstructural evolution of previously deformed AZ91D magnesium alloy during partial remelting, J. Alloys Compd. 477 (2009) 726–731.
[3] Jian-Yih Wang, Akhmad Saufan, P.H. Lin, H.Y. Bor, S. Lee, Y. Kawamura, Mechanical properties and strengthening behavior of Mg-Zn-MM alloy, Mater. Chem. Phys. 148 (2014) 28–31.
[4] Q. Chen, Z.X. Zhao, D.Y. Shu, Z.D. Zhao, Microstructure and mechanical properties of AZ91D magnesium alloy prepared by compound extrusion, Mater. Sci. Eng. A 528 (2011) 3930–3934.
[5] S.M. Fatemi-Varzaneh, A. Zarei-Hanzaki, J.M. Cabrera, P.R. Calvillo, EBSD characterization of repetitive grain refinement in AZ31 magnesium alloy, Mater. Chem. Phys. 149–150 (2015) 339–343.
[6] H. Hoche, H. Scheerer, D. Probst, E. Broszeit, C. Berger, Development of a plasma surface treatment for magnesium alloys to ensure sufficient wear and corrosion resistance, Surf. Coat. Technol. 174–175 (2003) 1018–1023.
[7] J.E. Gray, B. Luan, Protective coatings on magnesium and its alloys-a critical review, J. Alloys Compd. 336 (2002) 88–113.
[8] A. Seyfoori, Sh. Mirdamadi, Z.S. Seyedraoufi, A. Khavandi, M. Aliofkhazraei, Synthesis of biphasic calcium phosphate containing nanostructured films by micro arc oxidation on magnesium alloy, Mater. Chem. Phys. 142 (2013) 87–94.
[9] E.E. Demirci, E. Arslan, K.V. Ezirmik, Ö. Baran, Y. Totik, İ. Efeoglu, Investigation of wear, corrosion and tribocorrosion properties of AZ91 Mg alloy coated by micro arc oxidation process in the different electrolyte solutions, Thin Solid Films 528 (2013) 116–122.
[10] Y.K. Pana, C.Z. Chena, D.G. Wanga, Z.Q. Lina, Preparation and bioactivity of micro-arc oxidized calcium phosphate coatings, Mater. Chem. Phys. 141 (2013) 842–849.
[11] P. Shi, W.F. Ng, M.H. Wong, F.T. Cheng, Improvement of corrosion resistance of pure magnesium in Hanks' solution by microarc oxidation with sol-gel TiO_2 sealing, J. Alloys Compd. 469 (2009) 286–292.
[12] Z. Shi, G. Song, A. Atrens, The corrosion performance of anodised magnesium alloys, Corros. Sci. 48 (2006) 3531–3546.
[13] Y. Zhao, G.S. Wu, H.B. Pan, Kelvin W.K. Yeung, Paul K. Chu, Formation and electrochemical behavior of Al and O plasma-implanted biodegradable Mg-Y-RE alloy, Mater. Chem. Phys. 132 (2012) 187–191.
[14] H.X. Liu, Q. Xu, D.M. Xiong, B. Lin, C.L. Meng, Microstructure and corrosion resistance of AZ91D magnesium alloy treated by hybrid ion implantation and heat treatment, Vacuum 89 (2013) 233–237.
[15] Y. Zhao, G.S. Wu, Q.Y. Lu, J. Wu, R.Z. Xu, K.W.K. Yeung, P.K. Chu, Improved surface corrosion resistance of WE43 magnesium alloy by dual titanium and oxygen ion implantation, Thin Solid Films 529 (2013) 407–411.
[16] Y.J. Shi, S.Y. Long, S.C. Yang, F.S. Pan, Deposition of nano-scaled CrTiAlN multilayer coatings with different negative bias voltage on Mg alloy by unbalanced magnetron sputtering, Vacuum 84 (2010) 962–968.
[17] F. Hollstein, R. Wiedemann, J. Scholz, Characteristics of PVD-coatings on AZ31hp magnesium alloys, Surf. Coat. Technol. 162 (2003) 261–268.
[18] G.S. Wu, L.L. Sun, W. Dai, L.X. Song, A.Y. Wang, Influence of interlayers on corrosion resistance of diamond-like carbon coating on magnesium alloy, Surf. Coat. Technol. 204 (2010) 2193–2196.
[19] H. Hoche, C. Blawert, E. Broszeit, C. Berger, Galvanic corrosion properties of differently PVD-treated magnesium die cast alloy AZ91, Surf. Coat. Technol. 193 (2005) 223–229.
[20] N. Yamauchi, K. Demizu, N. Ueda, N.K. Cuong, T. Sone, Y. Hirose, Friction and wear of DLC films on magnesium alloy, Surf. Coat. Technol. 193 (2005) 277–282.
[21] N. Yamauchi, N. Ueda, A. Okamoto, T. Sone, M. Tsujikawa, S. Oki, DLC coating on Mg-Li alloy, Surf. Coat. Technol. 201 (2007) 4913–4918.
[22] G.W. Yi, F.Y. Yan, Mechanical and tribological properties of phenolic resin-based friction composites filled with several inorganic fillers, Wear 262 (2007) 121–129.
[23] M.H. Cho, J.J.S.J. Kim, H. Jang, Tribological properties of solid lubricants (graphite, Sb_2S_3, MoS_2) for automotive brake friction materials, Wear 260 (2006) 855–860.
[24] S. Betancourt, L.J. Cruz, A. Toro, Effect of the addition of carbonaceous fibers on the tribological behavior of a phenolic resin sliding against cast iron, Wear 272 (2011) 43–49.
[25] G.S. Wu, W. Dai, H. Zheng, A.Y. Wang, Improving wear resistance and corrosion resistance of AZ31 magnesium alloy by DLC/AlN/Al coating, Surf. Coat. Technol. 205 (2010) 2067–2073.
[26] Z.W. Xie, Z.Z. Luo, Q. Yang, T. Chen, S. Tan, Y.J. Wang, Y.M. Luo, Improving anti-wear and anti-corrosion properties of AM60 magnesium alloy by ion implantation and Al/AlN/CrAlN/CrN/MoS_2 gradient duplex coating, Vacuum 101 (2014) 171–176.
[27] W. Yang, P.L. Ke, Y. Fang, H. Zheng, A.Y. Wang, Microstructure and properties of duplex (Ti:N)-DLC/MAO coating on magnesium alloy, Appl. Surf. Sci. 270 (2013) 519–525.
[28] L.P. Wang, L. Huang, Z.W. Xie, X.F. Wang, B.Y. Tang, Fourth-generation plasma immersion ion implantation and deposition facility for hybrid surface modification layer fabrication, Rev. Sci. Instrum. 79 (2008) 023306.
[29] H. Cheng, Y. Sun, P. Hing, Microstructure evolution of AlN films deposited under various pressures by RF reactive sputtering, Surf. Coat. Technol. 166 (2003) 231–236.
[30] P.H. Mayrhofer, D. Music, Th Reeswinkel, H.G. Fu, J.M. Schneider, Structure, elastic properties and phase stability of $Cr_{1-x}Al_xN$, Acta Mater. 56 (2008) 2469–2475.
[31] D.H. Yu, C.Y. Wang, X.L. Cheng, F.L. Zhang, Microstructure and properties of TiAlSiN coatings prepared by hybrid PVD technology, Thin Solid Films 517 (2009) 4950–4955.
[32] C.L. Chang, J.W. Lee, M.D. Tseng, Microstructure, corrosion and tribological behaviors of TiAlSiN coatings deposited by cathodic arc plasma deposition, Thin Solid Films 517 (2009) 5231–5236.
[33] D.S. Kong, H.T. Wang, J.J. Cha, M. Pasta, K.J. Koski, J. Yao, Y. Cui, Synthesis of MoS_2 and $MoSe_2$ films with vertically aligned layers, Nano Lett. 13 (2013) 1341–1347.
[34] D. Chen, D. Xu, J.J. Wang, B. Zhao, Y.F. Zhang, Influence of the texture on Raman and X-ray diffraction characteristics of polycrystalline AlN films, Thin Solid Flims 517 (2008) 986–989.
[35] T.W. Scharf, P.G. Kotula, S.V. Prasad, Friction and wear mechanisms in MoS_2/Sb_2O_3/Au nanocomposite coatings, Acta Mater. 58 (2010) 4100–4109.
[36] L.P. Wang, S.W. Zhao, Z.W. Xie, L. Huang, X.F. Wang, MoS/Ti multilayer deposited on 2Cr13 substrate by PIIID, Nucl. Instrum. Methods Phys. Res. Sect. B 266 (2008) 730–733.
[37] T. Bell, H. Dong, Y. Sun, Realising the potential of duplex surface engineering, Tribol. Int. 31 (1998) 127–137.
[38] G.S. Wu, X.Q. Zeng, G.Y. Yuan, Growth and corrosion of aluminum PVD-coating on AZ31 magnesium alloy, Mater. Lett. 62 (2008) 4325–4327.
[39] A. Pardo, P. Casajús, M. Mohedano, A.E. Coy, F. Viejo, B. Torres, E. Matykina, Corrosion protection of Mg/Al alloys by thermal sprayed aluminium coatings, Appl. Surf. Sci. 255 (2009) 6968–6977.
[40] G.S. Wu, K.J. Ding, X.Q. Zeng, X.M. Wang, S.S. Yao, Improving corrosion resistance of titanium-coated magnesium alloy by modifying surface characteristics of magnesium alloy prior to titanium coating deposition, Scr. Mater. 61 (2009) 269–272.